http://www.zju.edu.cn/jzus; E-mail: jzus@zju.edu.cn
ISSN 1009-3095 *Journal of Zhejiang University SCIENCE* V.4, No.4, P.407-414, July-Aug., 2003

Low frequency oscillatory flow in a rotating curved pipe*

CHEN Hua-jun (陈华军), ZHANG Ben-zhao (章本照), SU Xiao-yan (苏霄燕)

(*Department of Mechanics, Zhejiang University, Hangzhou 310027, China*)

†E-mail: mec_zbzq@emb.zju.edu.cn

Received Aug.8, 2002; revision accepted Sept.29, 2002

Abstract: The low frequency oscillatory flow in a rotating curved pipe was studied by using the method of bi-parameter perturbation. Perturbation solutions up to the second order were obtained and the effects of rotation on the low frequency oscillatory flow were examined in detail. The results indicated that there exists evident difference between the low frequency oscillatory flow in a rotating curved pipe and in a curved pipe without rotation. During a period, four secondary vortexes may exist on the circular cross-section and the distribution of axial velocity and wall shear stress are related to the ratio of the Coriolis force to centrifugal force and the axial pressure gradient.

Key words: Oscillatory flow, Secondary flow, Perturbation method, Rotating pipe
Document code: A **CLC number:** 0357.1

INTRODUCTION

The motion of the flow in a rotating curved pipe is a fundamental problem, whose solution has potential applications in gas turbines, electric generators, electric motors and some equipments used in separation processes. It is important to know the flow structure characteristics when designing rotating machines.

As an interesting problem, the flow in rotating pipes had been studied by numerous authors, whose works focused on the circular or rectangular duct. Ludwieg (1951) was the first researcher to analyze the flow in rotating curved rectangular ducts and developed a solution based on the integral method. Miyazaki (1971) examined the secondary flow and heat transfer in a curved circular pipe with positive rotation. Ito and Motai (1974) first examined both co- and counter-rotation cases and found reversal of the secondary flow direction. Ito (1987) also conducted finite-difference computations and experiments on this problem. Daskopoulos and Lenhoff (1990), using orthogonal collocation, presented results of their bifurcation study of this combined problem in a circular pipe. In the most recent studies on this problem, Selmi *et al*. (1994) foucused on the bifurcation structure of the flow in a rotating duct with square cross section. Ishigaki (1996) studied the flow structure and the friction of a rotating circular pipe with small curvature, and defined a new parameter which is the ratio of the Coriolis force to the centrifugal force. Yamamoto *et al*. (2000) numerically studied the combined effects of rotation, torsion and curvature on the flow. Zhang *et al*. (2000; 2001a; 2001b) also examined the flow structure and the friction factor in a rotating curved circular, annular and rectangular pipe by theoretical and numerical methods.

However, most fluid flows in the rotating systems encountered in industrial applications are unsteady. The studies on unsteady flow in curved pipes initiated by Lyne (1971) have attracted interest not only for their engineering applications to heat exchangers and chemical reactors, but also for their relevance to hemodynamical problems (Pedley, 1980). These studies are mainly concentrated on the non-rotation cases, such as those reported by Simth (1975), Lin and Tarbell (1980), Hamakiotes and Beger (1990), Lynch *et al*. (1996), Zabielski and Mestel (1998), Waters and Pedley (1999).

To the authors' knowledge, there are no re-

* Project (No: 10272096) supported by the National Natural Science Fundation of China

ports on the unsteady flow in a rotating curved pipe probably because of the complexities of the problem. So it is quite necessary and useful to investigate the unsteady flow in rotating helical pipes. In this work, the unsteady low frequency oscillatory flow in a circular cross section pipe with small curvature was studied by applying bi-parameter method of perturbation and the solutions developed the results of Mullin and Greated (1980). Our emphasis were on the effect of rotation on the low frequency oscillatory flow yielded many new and interesting conclusions were obtained.

GOVERNING EQUATIONS

Fig.1 shows the rotating curved pipe and the coordinate system used in the paper. The coordinates are r^*, θ, s^*, where s^* is the centerline of the pipe. The radius of the pipe is R_c. The velocities in the directions of r^*, θ, s^* are denoted by u^*, v^*, w^*. The following dimensionless parameters are introduced:

$(s, r) = (s^*, r^*)/R_c$,

$(u, v, w) = (u^*, v^*, w^*)R_c/\upsilon$,

$P = p^* R_c^2/\rho\upsilon^2$,

$\Omega = (\Omega^* RR_c)/\upsilon$, $\kappa = \kappa^* R_c$, $t = \omega t^*$,

$\alpha = R_c(\omega/\upsilon)^{1/2}$,

$Re = 2w_m^* R_c/\upsilon$.

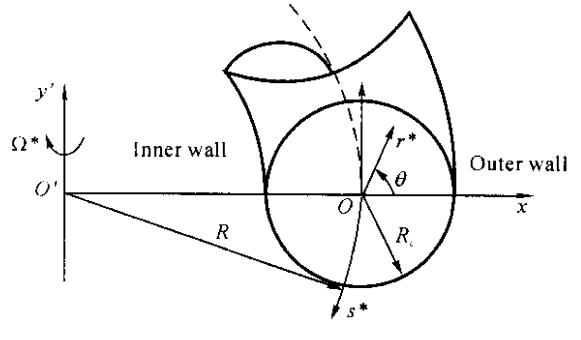

Fig.1 The rotating curved pipe and the coordinate system

Where p is dimensionless axial pressure, ω is the oscillating frequency, α is the Womersley Number, Ω is dimensionless constant angular velocity respectively (when $\Omega > 0$, that is the rotation has the same direction as the direction of s^*), κ is the dimensionless curvature, υ is the kinematic viscosity. It is assumed that the fluid flow is unsteady, laminar, hydrodynamically developed. According to Ishigaki (1996), for the pipe rotating at constant angular velocity about the y'-axis, the dimensionless continuity equation and N-S equations for a small curvature are given as:

$$\frac{\partial}{\partial r}(ru) + \frac{\partial v}{\partial \theta} = 0 \tag{1}$$

$$\alpha^2 \frac{\partial u}{\partial t} + u\frac{\partial u}{\partial r} + \frac{v}{r}\frac{\partial u}{\partial \theta} + \frac{v^2}{r} = -\frac{\partial P}{\partial r} + \kappa(w^2 + 2\Omega w)\cos\theta + \nabla^2 u - \frac{u}{r^2} - \frac{2}{r}\frac{\partial v}{\partial \theta} \tag{2}$$

$$\alpha^2 \frac{\partial v}{\partial t} + u\frac{\partial v}{\partial r} + \frac{v}{r}\frac{\partial v}{\partial \theta} + \frac{uv}{r} = -\frac{\partial P}{r\partial \theta} - \kappa(w^2 + 2\Omega w)\sin\theta + \nabla^2 v - \frac{v}{r^2} + \frac{2}{r}\frac{\partial u}{\partial \theta} \tag{3}$$

$$\alpha^2 \frac{\partial w}{\partial t} + u\frac{\partial w}{\partial r} + \frac{v}{r}\frac{\partial w}{\partial \theta} = -\frac{\partial P}{\partial s} - \kappa(2\Omega u\cos\theta - 2\Omega v\sin\theta) + \nabla^2 w \tag{4}$$

where $\nabla^2 = \frac{1}{r}\frac{\partial}{\partial}\left(r\frac{\partial}{\partial r}\right) + \frac{1}{r^2}\frac{\partial^2}{\partial \theta}$, and P is the reduced pressure defined by

$$P = p - \frac{1}{2}\Omega^2(1 + \kappa r\cos\theta)^2.$$

Define the axial pressure gradient to be

$$\frac{\partial P}{\partial s} = -G\cos t \tag{5}$$

where G is a positive constant.

A stream function $\psi = \psi(r, \theta)$, which automatically satisfies the continuity Eq.(1), may be defined according to

$$u = \frac{1}{r}\frac{\partial \psi}{\partial \theta}, \quad v = -\frac{\partial \psi}{\partial r} \tag{6}$$

Substituting Eq.(6) into Eqs.(2) and (3) and removing the terms of pressure, yields the equation of the stream function

$$-\alpha^2 \frac{\partial}{\partial t}(r\nabla^2\psi) + \left(-\frac{\partial \psi}{\partial \theta}\frac{\partial}{\partial r} + \frac{\partial \psi}{\partial r}\frac{\partial}{\partial \theta}\right)\nabla^2\psi = -\kappa r\frac{\partial(w^2 + \Omega w)}{\partial r}\sin\theta - \kappa\frac{\partial(w^2 + \Omega w)}{\partial \theta}\cos\theta - r\nabla^4\psi \tag{7}$$

Substituting Eq.(6) into Eq.(4), yields

$$\alpha^2\frac{\partial w}{\partial t}+\frac{1}{r}\frac{\partial\psi}{\partial\theta}\frac{\partial w}{\partial r}-\frac{1}{r}\frac{\partial\psi}{\partial r}\frac{\partial w}{\partial\theta}=G\cos t-\kappa\left(\frac{2\Omega}{r}\frac{\partial\psi}{\partial\theta}\cos\theta+\frac{2\Omega}{r}\frac{\partial\psi}{\partial r}\sin\theta\right)+\nabla^2 w \quad (8)$$

The boundary conditions are:

$$w=\psi=u=v=0,\frac{\partial\psi}{\partial r}=0 \text{ at } r=1 \quad (9)$$

According to Ishigaki (1996), the maximal body force ratio F, which represents the maximal ratio of the Coriolis force to the centrifugal force when the axial pressure gradient reaches its maximum, is defined as:

$$F=\frac{\Omega^* R}{w_m^*}$$

Where w_m^* is the average axial velocity of the cross-section at the moment when the axial pressure gradient reaches its maximum.

PERTURBATION SOLUTIONS

It is assumed that the curvature κ and α^2 are small, $\kappa=\varepsilon\ll1$ and $\alpha^2=\eta\ll1$. So it is natural to choose κ and α^2 as the perturbation parameters. According to Mullin and Greated(1980), successive approximations to the solution can be determined by expanding ψ and w as

$$w=\sum_{i=0}^{n}\sum_{j=0}^{m}w_{i,j}(r,\theta,t)\varepsilon^i\eta^j,$$
$$\psi=\sum_{i=1}^{n}\sum_{j=0}^{m}\psi_{i,j}(r,\theta,t)\varepsilon^i\eta^j, \quad (10)$$

Substituting Eq. (10) into the equation Eqs. (7) and (8), we can obtain the perturbation equations of each order. Considering the boundary condition Eq. (9) and solving the perturbation equations, yields each order solutions as follows (the second-order solutions have been listed):

$$w_{0,0}(r,\theta,t)=\frac{1}{4}G(1-r^2)\cos(t)$$

$$w_{0,1}(r,\theta,t)=\left(\frac{1}{64}r^4G-\frac{1}{16}r^2G+\frac{3}{64}G\right)\cdot\sin(t)$$

$$w_{0,2}(r,\theta,t)=\left(\frac{1}{2304}r^6G-\frac{1}{256}r^4G+\frac{3}{256}r^2G-\frac{19}{2304}G\right)\cos(t)$$

$$\psi_{1,0}(r,\theta,t)=-\frac{1}{4608}Gr\sin(\theta)(r-1)^2\cdot(r+1)^2(r^2G-4G)\cos^2(t)+\frac{1}{192}Gr\sin(\theta)\cdot(r-1)^2(r+1)^2\Omega\cos(t)$$

$$\psi_{1,1}(r,\theta,t)=\left(\frac{1}{737280}Gr\sin(\theta)(r-1)^2\cdot(r+1)^2(-114r^2G+299G+13r^4G)\cdot\cos(t)+\frac{1}{737280}Gr\sin(\theta)(r-1)^2(r+1)^2\cdot(960\Omega-160r^2\Omega)\right)\sin(t)$$

$$\psi_{1,2}(r,\theta,t)=-\frac{1}{88473600}Gr\sin(\theta)(r-1)^2\cdot(r+1)^2(870r^4G-60r^6G+10950G-4950r^2G)\cos^2(t)-\frac{1}{88473600}Gr\sin(\theta)(r-1)^2(r+1)^2(21880\Omega+360\Omega r^4-4880r^2\Omega)\cdot\cos(t)-\frac{1}{88473600}Gr\sin(\theta)(r-1)^2(r+1)^2\cdot(-4276G+31r^6G-418r^4G+2133r^2G)$$

$$w_{1,0}(r,\theta,t)=-\frac{1}{737280}\cos(\theta)rG^2(r-1)\cdot(r+1)(19G-r^6G+9r^4G-21r^2G)\cos^3(t)-\frac{1}{737280}\cos(\theta)rG^2(r-1)(r+1)(40\Omega r^4-120r^2\Omega+120\Omega)\cos^2(t)$$

$$w_{1,1}(r,\theta,t)=\left(\frac{1}{176947200}\cos(\theta)rG^2(r-1)\cdot(r+1)(-39Gr^8+501r^6G-2349r^4G+4611r^2G-3984G)\cos^2(t)+\frac{1}{176947200}\cos(\theta)\cdot rG^2(r-1)(r+1)(-17200\Omega+1200\Omega r^6-8400\Omega r^4+18800r^2\Omega)\cos(t)\right)\sin(t)$$

$$w_{1,2}(r,\theta,t)=\frac{1}{14863564800}\cos(\theta)rG^2(r-1)\cdot(r+1)(110714r^4G-200716r^2G+4174Gr^8+171740G-30476r^6G-236r^{10}G)\cos^3(t)+\frac{1}{14863564800}\cos(\theta)rG^2(r-1)(r+1)\cdot(299292\Omega r^4-593348r^2\Omega+5292r^8\Omega+526792\Omega-66108\Omega r^6)\cos^2(t)+\frac{1}{14863564800}\cdot\cos(\theta)rG^2(r-1)(r+1)(120307r^2G-2683Gr^8-102440G+19367r^6G+152r^{10}G-67713r^4G)\cos(t)+\frac{1}{14863564800}\cos(\theta)rG^2\cdot(r-1)(r+1)(-136640\Omega r^4-2520r^8\Omega+$$

$$258160r^2\Omega + 32760\Omega r^6 - 224840\Omega)$$

$$\psi_{2,0}(r,\theta,t) =$$

$$\sin(2\theta)\sum_{j=0}^{2}\left(G^{4-j}\cos t^{(4-j)}\Omega^j\sum_{i=1}^{8-j}A_{ij}^{(1)}r^{2i}\right)$$

$$\psi_{2,1}(r,\theta,t) =$$

$$\sin(2\theta)\sin(t)\sum_{j=0}^{2}\left(G^{4-j}\cos t^{(3-j)}\Omega^j\sum_{i=1}^{8-j}A_{ij}^{(2)}r^{2i}\right)$$

$$\psi_{2,2}(r,\theta,t) =$$

$$\sin(2\theta)\sum_{j=0}^{2}\left(G^{4-j}\cos t^{(4-j)}\Omega^j\sum_{i=1}^{9-j}A_{ij}^{(3)}r^{2i} + G^{4-j}\cos t^{(2-j)}\Omega^j\sum_{i=1}^{9-j}A_{ij}^{(4)}r^{2i}\right)$$

$$w_{2,0}(r,\theta,t) =$$

$$\sum_{k=0}^{1}\left(\cos(2\theta)^{(1-k)}\left(\sum_{j=0}^{2}G^{5-j}\cos t^{(5-j)}\Omega^j\sum_{i=1}^{8-j}B_{ij}^{(1)}r^{2i} + \sum_{j=0}^{1}G^{2-j}\cos t^{(2-j)}\Omega^{j+1}\sum_{i=1}^{4-j}B_{ij}^{(2)}r^{2i}\right)\right)$$

$$w_{2,1}(r,\theta,t) =$$

$$\sin(t)\sum_{k=0}^{1}\left(\cos(2\theta)^{(1-k)}\left(\sum_{j=0}^{2}G^{5-j}\cos t^{(4-j)}\Omega^j\cdot\sum_{i=1}^{9-j}B_{ij}^{(3)}r^{2i} + \sum_{j=0}^{1}G^{2-j}\cos t^{(1-j)}\Omega^{j+1}\sum_{i=1}^{5-j}B_{ij}^{(4)}r^{2i}\right)\right)$$

$$w_{2,2}(r,\theta,t) =$$

$$\sum_{k=0}^{1}\left(\cos(2\theta)^{(1-k)}\left(\sum_{j=0}^{2}G^{5-j}\cos t^{(5-j)}\Omega^j\sum_{i=1}^{10-j}B_{ij}^{(5)}r^{2i} + \sum_{j=0}^{2}G^{5-j}\cos t^{(5-j)}\Omega^j\sum_{i=1}^{9-j}B_{ij}^{(6)}r^{2i}\right)\right) +$$

$$G\cos(4\theta)\Omega^2\sum_{i=1}^{4}C_ir^{2i} + G^2\cos(2\theta)\Omega\sum_{i=1}^{6}D_ir^{2i} + G^2\Omega\sum_{i=1}^{6}E_ir^{2i}$$

The coefficients $A_{ij}^{(k)}$, $B_{ij}^{(k)}$, C_i, D_i, E_i are integral constants. To make the paper compact, the expressions of the coefficients have not been shown here. When $\alpha = 0$, the solutions above have the same expressions as those of Zhang *et al*. (2000). According to the suggestion of Van Dyke (1978), Mullin and Greated (1980), the solution is convergent up to the Dean number $D_n < 576$ ($D_n = \kappa Re^2$, $Re = G/4$) and $\alpha \approx 1.5$, therefore, the region of validity of the solution can be expressed as

$$\kappa < \frac{576}{2Re^2} = \frac{4608}{G^2}, \alpha < 1.5$$

We have successfully solved low frequency oscillatory flow in a rotating curved pipe by applying bi-parameter perturbation method and obtained the fully second order solutions. Substituting solutions of the stream function ψ into Eq. (6), we can obtain the velocity expressions of the secondary flow concretely.

RESULTS AND DISCUSSION

A remarkable property of the flow in a rotating curved pipe of the motion is the presence of centrifugal and Coriolis forces which cause two kinds of secondary flows in the cross section perpendicular to the axial velocity (normal cross section). In order to determine the effects of rotation on the flow, we keep G, κ, and α as constants in this paper and study the flow structures for different F to check the effects of rotation on the oscillatory flow. In the contour figures, the dotted lines denote negative values, the upper part of the cross section is the secondary flow and the lower is the axial velocity. The outer side is on the right for all the contours.

1. The development of flow pattern

Fig. 2 shows the secondary flow streamlines and axial velocity contours without rotation. ($G = 200$, $\kappa = 0.1$, $\alpha = 0.2$, $F = 0$, $\psi_{\max}$, which represents the intensity of the secondary flow (Ito *et al*., 1974) and locates at the center of secondary flow vortex, is the maximum of the stream function, $w_{\max}$ and $w_{\min}$ are the maximal and minimal values of axial velocity, respectively). For the case $F = 0$, the Coriolis force has no effect and the centrifugal force contributes on the flow. During the entire period, a vortex caused by centrifugal force maintains almost a constant profile and the maximum of the axial velocity always shifts to the outer wall. This can be easily understood if we realize that no matter how the axial pressure gradient changes, the centrifugal force always points to the outer bend. When t approaches to 1.58, the axial pressure gradient almost becomes zero and then shift to a negative value. At this moment, the intensity of secondary flow and the flux almost reaches to zero.

Fig. 3 shows the variation of flow pattern with t for $F > 0$. For the case $F = 3$, when $t = 0$ and $t = 0.78$, a positive secondary vortex can be found in the upper half contours and the center of the maximum axial flow is close to the outer

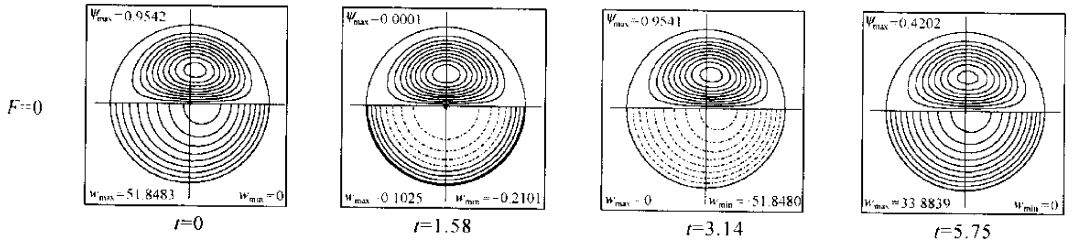

Fig.2 Secondary flow streamlines and axial velocity contours for $G=200$, $\kappa=0.1$, $\alpha=0.2$

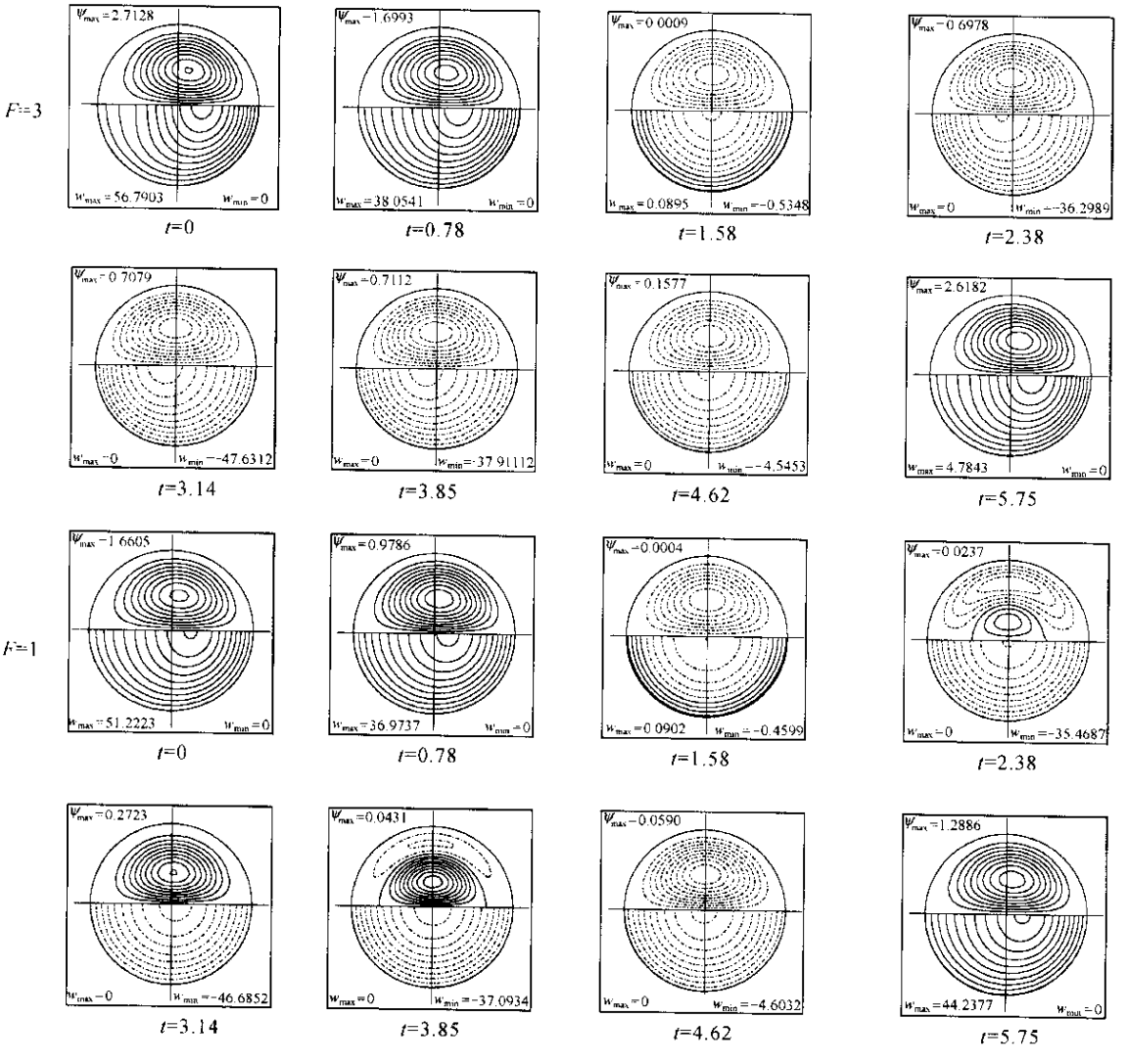

Fig.3 Secondary flow streamlines and axial velocity contours for $G=200$, $\kappa=0.1$, $\alpha=0.2$

wall. At this moment, the effect of Coriolis force just intensified the secondary flow because the Coriolis force has the same direction as that of the centrifugal force. When t approaches to 1.58, the stream function becomes a negative value and negative axial velocity is generated on the cross-section. When $t=2.38$, the negative axial velocity contour lines take up the whole cross-section. At this moment, the Coriolis force has direction opposite to that of the centrifugal

force due to the negative axial velocity and the inward Coriolis force exerts the main effect on the flow. So the reversal flow pattern can be found in the cross-section for the cases $t = 2.38$ -4.62. When $t = 5.75$, the stream function value and axial velocity return to positive due to the outward Coriolis force and centrifugal force. For the case $F = 1$, when $t = 0$ and $t = 0.78$, the flow pattern is similar to that of the case $F = 3$. But when $t = 2.38$, a new vortex caused by the Coriolis force is generated near the center and the distribution of axial velocity is similar to that of Poiseuillle flow. The reason for this flow structure is that the inward Coriolis force almost balances the outer centrifugal force at this moment. When $t = 3.14$, the new vortex takes up the whole cross-section. The flow pattern, which is similar to that of case $t = 2.38$, can also be found at $t = 3.85$.

Fig.4 shows the variation of flow pattern with t for $F < 0$. For the case $F < 0$, it means that when the axial velocity is positive, the Coriolis force has direction opposite to that of the centrifugal force. So for the case $F = -3$, when $t = 0$, the negative stream function can be found in the upper part of the cross-section due to the inward Coriolis force and the maximum of the axial flow shifts to the inner wall. When $t = 1.73$ and $t = 3.14$, the axial velocity becomes to negative and the effect of the Coriolis force just intensified the secondary flow. For the case $F = -3$, when the inward Coriolis force momentarily almost counteracts the outer centrifugal force , two-vortex structure can be found in the upper half of the cross-section.

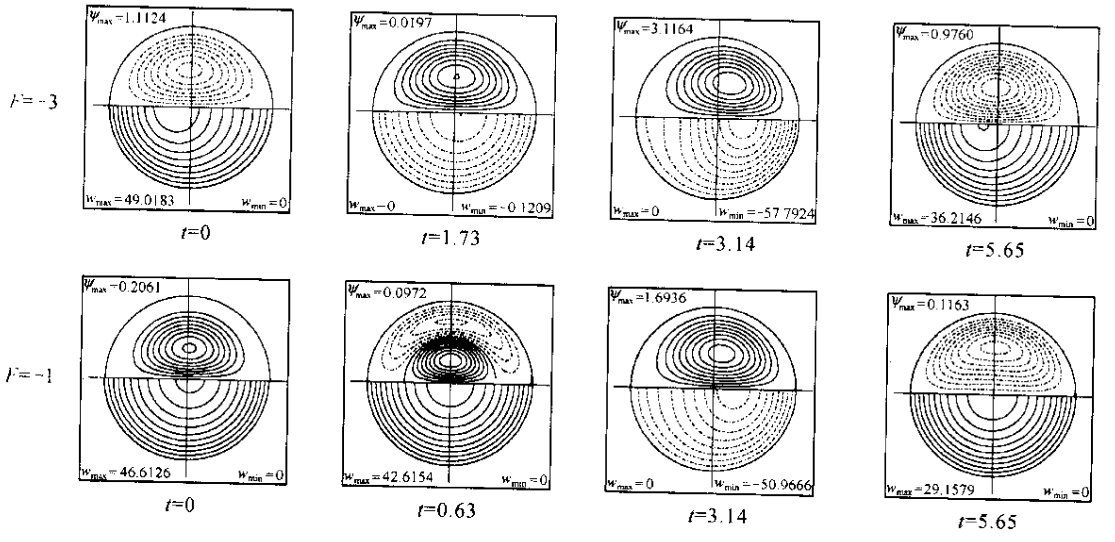

Fig.4 Secondary flow streamlines and axial velocity contours for $G = 200$, $\kappa = 0.1$, $\alpha = 0.2$

The variation of the stream function maximum ψ_{max} with t is shown in Fig.5. For the case (a) $F \geqslant 0$, the figure indicates that when $t < \pi/2$, the intensity becomes weaker with the increasing of time due to the decreasing axial pressure gradient and for a given time, the larger F is, the stronger the intensity of the secondary flow will be. As t approaches $\pi/2$, the intensity almost becomes zero. When t is between $\pi/2 - 3\pi/2$, the Coriolis force has direction opposite to that of the centrifugal force. For the curve $F = 1$, we found that when t was about 2.4 and 3.8, the secondary flow had minimal intensity because the inward Coriolis force and the outward centrifugal force almost counteract each other. When $t > 3\pi/2$, the intensity of secondary flow becomes stronger as t further increases. For the case (b) $F < 0$, it was found that when $0 < t < \pi$ and $\pi < t < 2\pi$, the variation of the secondary flow intensity with t was similar to that of case (a) for $\pi < t < 2\pi$ and $0 < t < \pi$, respectively.

2. The wall shear stress

As friction factor is one of the important flow properties in engineering applications, it is necessary to check the properties of the friction factor in detail. The non-dimensional wall shear

stress is determined by the non-dimensional axial velocity at the point nearest to wall and is defined as follows:

$$\tau = \tau^* R_c^2/\rho\upsilon^2$$

where τ^* is the dimensional wall stress $\tau^* = \rho\upsilon\dfrac{\partial w^*}{\partial n}\bigg|_{\Gamma}$, Γ is the wall, n is the normal vector of the wall.

Fig.6 shows the distribution of the non-dimensional wall shear stress when the axial pressure gradient reaches to the maximum ($t = 0$, π). For case (a) $t = 0$ ($F > 0$), the maximum of wall shear stress locates at $\theta = 0$ (the outer wall) and the minimum locates at $\theta = \pi$ (the inner wall). When the rotation speed increases, the maximum of wall shear stress increases while the minimum decreases. In the Fig. 6 (c) $F < 0$, similar distribution can also be found

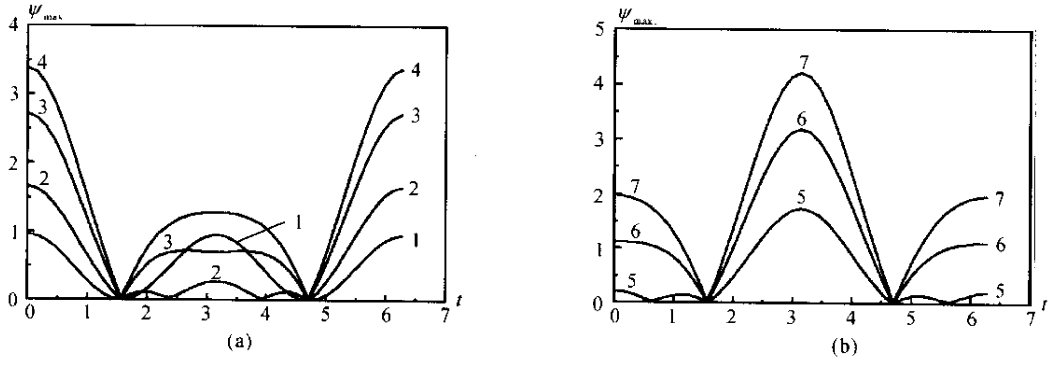

Fig.5 The variation of ψ_{max} with t for $G = 200$, $\kappa = 0.1$, $\alpha = 0.2$ (a) $F \geqslant 0$; (b) $F < 0$
(1: $F = 0$; 2: $F = 1$; 3: $F = 3$; 4: $F = 5$; 5: $F = -1$; 6: $F = -3$; 7: $F = -5$)

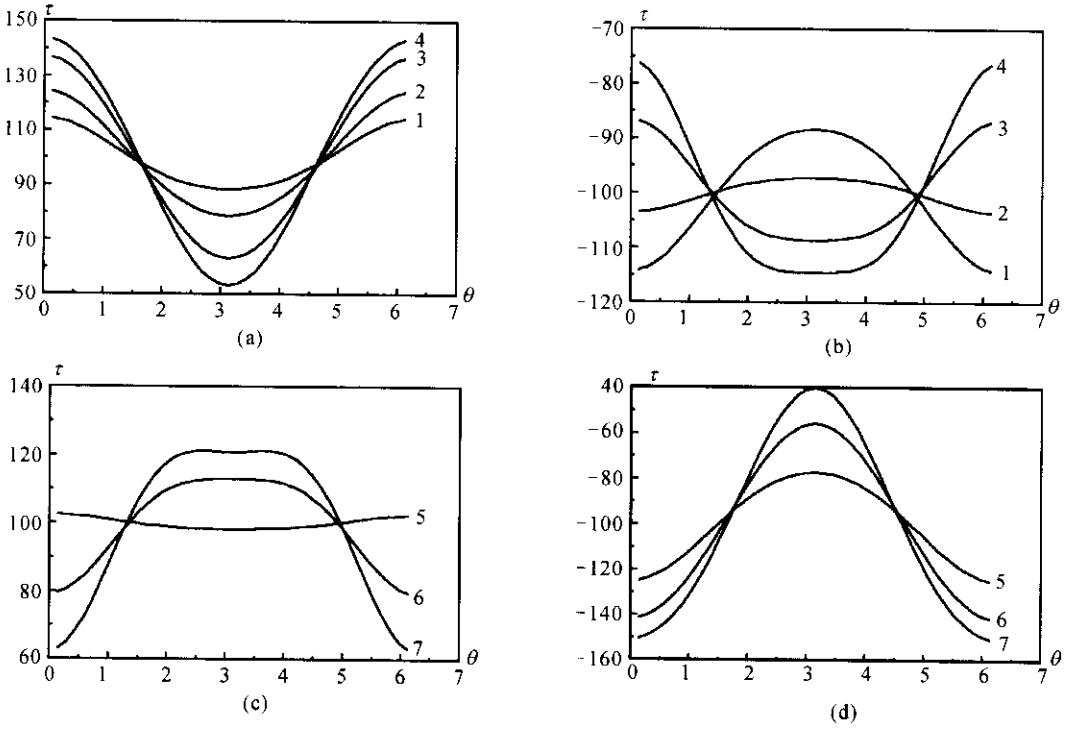

Fig.6 Fig.6 The distribution of τ at different t for $G = 200$, $\kappa = 0.1$, $\alpha = 0.2$
(a) $t = 0$ ($F > 0$); (b) $t = \pi$ ($F > 0$); (c) $t = 0$ ($F < 0$); (d) $t = \pi$ ($F < 0$)
(1: $F = 0$; 2: $F = 1$; 3: $F = 3$; 4: $F = 5$; 5: $F = -1$; 6: $F = -3$; 7: $F = -5$)

when $F = -1$. But as F decreases, the maximum of wall shear stress moves to the inner wall while the minimum shifts to the outer wall. When $t = \pi$, the direction of wall shear stress changes due to the negative pressure gradient. In the Fig. 6(b), $F > 0$, it shows that the wall shear stress near the outer wall becomes smaller gradually with the increasing of $|F|$, while for $|F < 0|$, the Fig. 6(d) shows that the wall shear stress near the outer wall increases with the increase of $|F|$.

CONCLUSIONS

Although the problem of the flow in rotating curved ducts had been studied previously by many authors, none of them focused on the oscillatory axial pressure gradient flow in a rotating curved pipe. This work aims to bridge this gap. In this paper, low frequency cosinoidal varying axial pressure gradient is imposed and the secondary order solutions of oscillatory flow in rotating curved pipes were obtained by the bi-parameter perturbation method.

For the stationary case ($F = 0$), the flow pattern maintains almost a constant profile during the entire period and the low frequency oscillatory axial pressure gradient has almost no effect on the structure of the flow pattern. But when the effect of rotation ($F \neq 0$) exists, the flow phenomena become more complicated. For a small (such as $F = -1$, $F = 1$), the inward Coriolis force momentarily almost balances the outer centrifugal force and at this moment, a new vortex caused by the Coriolis force can be found in the secondary flow pattern and the distribution of axial flow is similar to Poiseuillle flow. For larger F (such as $F = -3$, $F = 3$), the number of secondary vortex does not change for the whole period and the location of maximum of axial velocity is decided by the axial pressure gradient. The distribution of wall shear stress is related to the ratio of the Coriolis force to centrifugal force and the axial pressure gradient.

References

Daskopoulos, P. and Lenhoff, A.M., 1990. Flow in curved ducts. Part 2. Rotating ducts. *J. Fluid Mech.*, **217**: 575 – 593.

Hamakiotes, C.C. and Berger, S.A., 1990. Periodic flows through curved tube: the effect of the frequency parameter. *J. Fluid. Mech.*, **210**: 353 – 370.

Ishigaki, H., 1996. Flow in rotating curved pipes. *J. Fluid Mech.*, **329**: 373 – 388.

Ito, H. and Motai, T., 1974. Secondary flow in a rotating curved pipe. *Rep. Inst. High Speed Mech.*, **29**: 33 – 57.

Ito, H., 1987. Flow in curved pipe. *Japan Soc. Mech. Engng, Intl J.*, **30**: 543 – 552.

Komai, Y. and Tanishita, K., 1997. Fully developed intermittent flow in a curved tube. *J. Fluid Mech.*, **347**: 263 – 287.

Lin, J.J. and Tarbell, J.M., 1980. An Experimental and numerical study of periodic flow in a curved tube. *J Fluid Mech.*, **100**: 0623 – 638.

Lynch, D.G., Waters, S.L. and Pedley, T.J., 1996. Flow in a tube with non-uniform, time-dependent curvature: governing equations and simple example. *J. Fluid Mech.*, **323**: 237 – 265.

Lyne, W.H., 1971. Unsteady viscous flow in a curved pipe. *J. Fluid Mech.*, **45**: 13 – 31.

Ludwieg, H., 1951. Die Ausgebildete Kanalstromung in einem Rotierenden system. *Ingenieur-Archiv.*, **19**: 296 – 308.

Miyazaki, H., 1971. Combined free and forced convective heat transfer and fluid flow in rotating curved circular tube. *Intl J. Heat Mass Transfer.*, **14**: 1295 – 1309.

Mullin, T. and Greated, C.A., 1980. Oscillatory flow in curved pipes. Part II. The fully-developed case. *J. Fluid Mech.*, **98**: 397 – 416.

Pedley, T.J., 1980. The fluid mechanics of large blood vessel. Cambridge University Press, Cambidge.

Selmi, M., Nandakumar, K. and Finlay, W.H., 1994. A bifurcation study of viscous flow through a rotating curved pipe. *J. Fluid Mech.*, **262**: 353 – 375.

Smith, F.T., 1975. Pulsatile flow in curved pipes. *J. Fluid Mech.*, **71**: 15 – 42.

Van Dyke, M., 1978, Extended Stokes Series: Laminar Flow through aloosely Coiled Pipe. *J. Fluid. Mech.*, **86**: 129 – 145.

Waters, S.L. and Pedley, T.J., 1999. Oscillatory flow in a tube of time-dependent curvature. Part 1. Perturbation to flow in a stationary curved tube. *J. Fluid Mech.*, **383**: 327 – 352.

Yamamoto, K., Alam, M.D., Yasuhara, J. and Aribwo, A., 2000. Flow through a rotating helical pipe with circular cross-section. *Int. J. heat and fluid flow*, **21**: 213 – 220.

Zabielski, L. and Mestel, A.J., 1998. Unsteady blood flow in a helically symmetric pipe. *J. Fluid Mech.*, **370**: 321 – 345.

Zhang, J.S., Shen, X.R. and Zhang, B.Z., 2000. Fluid Flow in a Rotating Curved pipe. *Journal of Hydrodynamics. Ser. B.*, **12**(1): 108 – 116.

Zhang, B.Z., Chen, Q., Zhang. J.S. and Cui, L.C., 2001a. The perturbation Solutions of the Flow in a Rotating Curved Annular Pipe. *J. of Hydrodynamics, Ser. B.* **13**(1): 75 – 80.

Zhang, J.S., Zhang, B.Z. and Ju, J.W., 2001b. Fluid flow in rotating curved rectangular duct. *Int J. Heat Fluid Flow*, **22**: 583 – 592.